ACS APPLIED BIO MATERIALS

www.acsabm.org Article

Enhanced Functional Properties of Three DNA Origami Nanostructures as Doxorubicin Carriers to Breast Cancer Cells

Anuttara Udomprasert,* Chanida Wootthichairangsan, Ratchanee Duangrat, Supattra Chaithongyot, Yuwei Zhang, Rachel Nixon, Wenyan Liu, Risheng Wang, Mathurose Ponglikitmongkol, and Thaned Kangsamaksin*

Cite This: *ACS Appl. Bio Mater.* 2022, 5, 2262−2272 Read Online

ACCESS | Metrics & More | Article Recommendations | Supporting Information

ABSTRACT: Previous studies have shown that chemotherapeutic efficacy could be enhanced with targeted drug delivery. Various DNA origami nanostructures have been investigated as drug carriers. Here, we compared drug delivery functionalities of three similar DNA origami nanostructures, Disc, Donut, and Sphere, that differ in structural dimension. Our results demonstrated that Donut was the most stable and exhibited the highest Dox-loading capacity. MUC1 aptamer modification in our nanostructures increased cellular uptake in MUC1-high MCF-7. Among the three nanostructures, unmodified Donut exerted the highest Dox cytotoxicity in MCF-7, and MUC1 aptamer modification did not further improve its effect, implicating that Dox delivery by Donut was efficient. However, all Dox-loaded nanostructures showed comparable cytotoxicity in MDA-MB-231 due to the innate sensitivity of this cell line to Dox. Our results successfully demonstrated that functional properties of DNA origami nanocarriers could be tuned by structural design, and three-dimensional Donut appeared to be the most efficient nanocarrier.

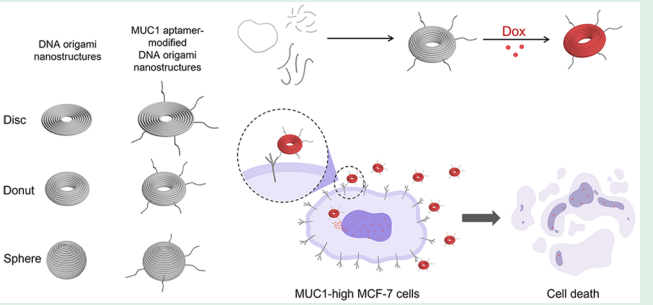

KEYWORDS: *DNA origami nanostructures, drug delivery system, doxorubicin, MUC1 aptamer, enhanced specificity*

INTRODUCTION

Chemotherapy is a common treatment for cancer patients to cure cancer or reduce its symptoms by using anticancer drugs. These therapeutic agents interfere with basic biochemical pathways necessary for cell viability, such as DNA replication and protein translation, and eventually result in cancer cell death. However, they exert nonspecific cytotoxic effects on normal proliferating cells, which lead to adverse effects of chemotherapy. For instance, doxorubicin (Dox), a widely used anthracycline antibiotic, can increase the risk of fatal cardiotoxicity.[1] To reduce side effects, targeted therapy and drug delivery systems have been developed to precisely deliver anticancer drugs only to cancer cells. Moreover, this could lead to a reduction in effectively required dosage drugs for patients. Different types of nanomaterials have been explored for smart nanocarrier construction including metals,[2] polymers,[3] lipid-polymer hybrids,[4] proteins,[5,6] and nucleic acids.[7−9]

To construct smart drug nanovehicles, DNA is an attractive starting material according to its own physical and chemical properties. Also, this molecule is naturally biocompatible and biodegradable. Structural DNA nanotechnology, founded by Nadrian C. Seeman, utilizes DNA as a building block for constructing nanostructures with precisely designed geometries and programmable functional modifications.[10] The scaffolded DNA origami technique is a breakthrough in structural DNA nanotechnology, enabling the formation of larger DNA nanostructures with a simple self-assembling step.[11] Previous studies have established powerful tools for automated design for any desired sizes and shapes of DNA origami nanostructures.[12−15] The production methods for customized single-stranded DNA scaffold synthesis with programmable sequence and length have been reported[16−18] as well as the efficient purification strategies.[19−21] In addition, it has been shown that spatially functional modification on DNA nanostructures at molecular levels could be achieved.[22−25]

Current applications of DNA origami nanostructures include protein and cell engineering, diagnostics, and therapeutics such as drug and gene delivery. It has been widely shown that not only did DNA origami nanocarriers enhance therapeutic efficacy but also they overcame drug resistance in several cases.[7,8] Previous reports demonstrated that triangular DNA origami nanostructures offer a promising platform for Dox

Received: February 9, 2022
Accepted: April 20, 2022
Published: May 2, 2022

https://doi.org/10.1021/acsabm.2c00114
ACS Appl. Bio Mater. 2022, 5, 2262−2272

delivery both *in vitro* and *in vivo*.[7,9] Similar to Dox, a rod-like DNA origami nanostructure was tested as a daunorubicin nanovehicle to circumvent drug resistance in leukemic cells.[26] In addition to chemotherapeutic agents, CpG motifs were delivered as immunostimulants using a DNA origami nanotube.[27] DNA origami in a barrel-like shape was constructed as a logic-gated nanorobot for antibody fragment transport.[28] Recently, researchers have demonstrated that the triangular, tubular, and rectangular shaped DNA origami nanostructure was utilized as a carrier platform for combined drug and gene therapy.[29−32] In addition, as drug carriers for transdermal drug delivery using a mouse melanoma model, DNA origami nanostructures could enhance drug accumulation and tumor inhibition compared with liposomes and polymeric nanoparticles.[33] Researchers also found that these DNA origami nanostructures are nontoxic even at high concentration (1 μg/mL).

To enhance target selectivity, the targeted drug delivery system could be constructed using a specific targeting ligand modification onto the nanocarriers. Aptamers have attracted much attention as a promising targeting agent. They are short single-stranded DNA or RNA that specifically bind to target molecules like antibodies. After binding with receptors on cell surface, aptamers are endocytosed into cells mostly via clathrin-mediated pathways.[34] In addition, they are easily modified onto DNA nanostructures to facilitate the selective uptake into specific cells. MUC1 aptamer is a widely used targeting ligand specifically binding to mucin 1 glycoproteins (MUC1) overexpressed on the cell surface of several types of cancer cells.[35,36] According to our previous reports, MUC1-modified DNA nanosphere could differently respond to lysates of cells with MUC1-positive cells, MCF-7 cells, and MUC1-negative cells, MDA-MB-231 cells.[37] Moreover, the specificity of MUC1-modified DNA nanosphere had been determined against three cell lines with different expression levels of MUC1 proteins.[38] Our results clearly showed that aptamer modification can selectively enhance intracellular internalization of DNA origami nanostructures into targeted cells. Several studies showed the specific targeting efficiency of MUC1-modified DNA nanostructure in targeted drug delivery to MCF-7 cells.[29,30,32,38−40] Also, it has been shown that the amount of targeting ligands on nanocarriers may affect cellular uptake efficiency.[41,42]

During the past decade, DNA origami nanostructures in various sizes and shapes, such as nanotube,[27,31,43] nanorod,[7,26,44] triangle,[7,9,29,30] rectangle,[32] and sphere,[37,38,45] have been demonstrated as drug delivery vehicles. Several studies have demonstrated that the cellular internalization of DNA origami nanostructures depends on size, shape, and even cell lines.[46−49] DNA origami nanostructures that are compact and have a low aspect ratio in the size of 50−80 nm are better for cellular internalization.[33] Also, different shapes of DNA origami nanostructures offer different drug loading and releasing capabilities.[50] Even though several studies showed that the size and shape of DNA origami nanocarriers might have some effects on functional properties as drug delivery vehicles,[33,44,46−53] those previous reports mostly compared the DNA nanostructures with different sizes and shapes. Moreover, some of those nanostructures are quite unique in their structural design strategy. On the basis of original scaffold DNA origami method, these DNA origami nanostructures are designed with the scaffold folding to form planar structures with a height of one-helix layer.[11] Similar to the original one, DNA nanostructures with complex curved surface could be obtained by designing the pattern of crossovers to get the out-of-plane curvature.[45] Another design is called the honeycomb-pleat-based strategy, which leads to the densely packed brick-like DNA origami nanostructures with a height of multihelix layer.[54] Alternatively, the structural design rule for the construction of complex 3D nanocage-like wireframe DNA origami nanostructures had also been reported.[55] It has been known that the formation of DNA origami nanostructures can be done in an one-pot annealing process. However, the annealing protocols for each DNA origami nanostructure are different in detail. The original and curve-surfaced DNA origami nanostructures could be annealed in a simple thermocycler within a few hours. The densely packed and wireframe DNA origami nanostructures require high-performance thermocycler equipment since the temperature needs to be slowly cooled down over a long period of time. This is a limitation in the construction of DNA origami nanostructures with complex DNA folding. In this study, we aimed to focus on similar shape DNA origami nanostructures that could be easily annealed in simple thermocycler equipment. Three similar shapes of nanostructures that differ in structural dimension were selected for comparative study on functional properties as nanovehicles. Disc nanostructure is a two-dimensional (2D) structure, while Donut and Sphere are three-dimensional (3D) structures. The drug delivery properties of these DNA origami nanostructures including stability, drug loading and releasing capacity, cellular uptake, and cytotoxicity were investigated. Also, the specificity of these DNA origami nanostructures after aptamer modification was examined.

EXPERIMENTAL SECTION

Materials. All single-stranded oligonucleotides and Cy5-modified oligonucleotides were purchased from Integrated DNA Technologies Pte. Ltd. (Singapore), and M13mp18 was obtained from Bayou Biolab (USA). Doxorubicin (Dox) was purchased from Sigma-Aldrich (USA). The MCF-7 and MDA-MB-231 cells were maintained in our laboratory. Dulbecco's modified Eagle's medium (DMEM), fetal bovine serum (FBS), penicillin, and streptomycin were purchased from Thermo Fisher Scientific Inc. (USA). Mouse anti-mucin1 antibody (primary antibody), rabbit antimouse antibody (secondary antibody) labeled with horseradish peroxidase (HRP), FITC-conjugated antimouse antibody (secondary antibody), β-actin, Hoechst 33342, and phalloidin were purchased from Cell Signaling Technology (USA). Clarity Western ECL substrate was purchased from Bio-Rad (USA).

Preparation of DNA Origami Nanostructures. The staple strands for the assembly of DNA origami nanostructures into three different shapes, Disc, Donut, and Sphere, were modified according to Han's report.[45] These DNA origami nanostructures were formed using a method from our previous study.[37,38] Briefly, all DNA strands (scaffold and staples) were mixed together in 1X TAE/Mg^{2+} buffer (40 mM Tris; 20 mM acetic acid; 2 mM EDTA; and 12.5 mM magnesium acetate), and the mixture was annealed in a thermocycler by gradually cooling from 68 to 25 °C at 0.6 °C/min and from 25 to 4 °C at 1 °C/min. After an annealing step, DNA origami nanostructures were purified using PEG purification method.[19] Each sample was mixed with PEG8000 purification buffer and then centrifuged at 13 000 rpm at 16 °C for an hour. The supernatant was discarded to remove the excess staple strands and the pellet was resuspended in TAE/Mg^{2+} buffer.

Characterization of DNA Origami Nanostructures. The annealed DNA origami nanostructures were analyzed by a 1.5% agarose gel containing 16 mM $MgCl_2$ at 75 V in 0.5X TBE buffer (22.25 mM Tris; 22.25 mM boric acid; and 0.5 mM EDTA) containing 11 mM $MgCl_2$. The gel was stained with ethidium bromide

https://doi.org/10.1021/acsabm.2c00114
ACS Appl. Bio Mater. 2022, 5, 2262−2272

Scheme 1. Structural Design of Aptamer-Modified Dox-Loaded DNA Origami Nanostructures as Targeted Drug Delivery System[1]

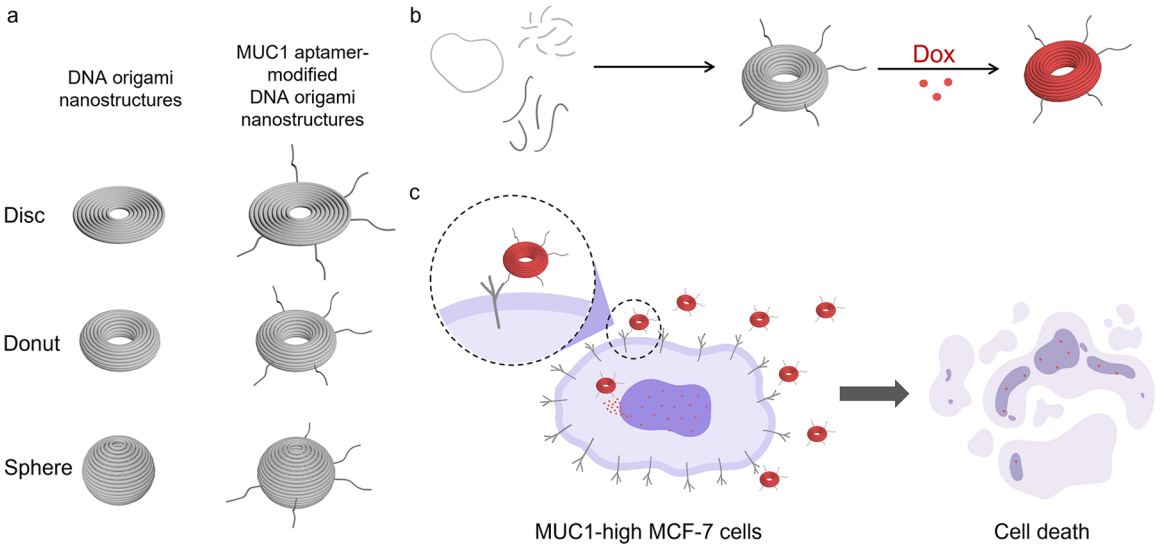

[1](a) Diagrams of DNA origami nanostructures, Disc, Donut, and Sphere, with and without MUC1 aptamer modification. (b) Self-assembled Dox-loaded DNA origami nanocarriers. (c) Dox-loaded MUC1-modified DNA origami nanostructures as targeted nanocarriers to specific cancer cells.

before visualization. The annealed DNA origami nanostructures were characterized by atomic force microscopy (AFM). The samples were deposited onto freshly cleaved mica (Ted Pella, Inc., USA) for 5 min and then washed with distilled water twice and air-dried. AFM imaging was performed with a tapping in air mode using ScanAsyst-Air silicon nitride cantilever. The annealed DNA origami nanostructures were also characterized by transmission electron microscopy (TEM). After the samples were deposited onto a negatively glow-discharged carbon-coated grid for 3 min, the excess solution was wicked using a filter paper. Then 0.7% uranyl acetate solution was added for 45 s to negatively stain the samples and then wicked using a filter paper. After drying, TEM imaging was performed using a Tecnai F20 FEG transmission electron microscope operating at 120 kV in bright field mode.

Stability Assay. The stability of each DNA origami nanostructure was separately investigated by incubating these DNA nanostructures in the annealing buffer (1X TAE/Mg^{2+}) and cell culture media (DMEM supplemented with 10% FBS) at both room temperature and 37 °C. Next, the samples were analyzed on a 1.5% agarose gel containing 16 mM $MgCl_2$ at 75 V in 0.5X TBE buffer (22.25 mM Tris; 22.25 mM boric acid; and 0.5 mM EDTA) containing 11 mM $MgCl_2$. The gel was stained with ethidium bromide before visualization.

Doxorubicin Loading. *For Fluorescence Experiment.* DNA origami nanostructures at different concentrations (3−9 nM) were incubated with 10 μM Dox for 3 h. Then the fluorescence intensity of the samples was measured with the excitation wavelength at 470 nm and the emission wavelength ranging from 500 to 750 nm using fluorescence spectrophotometer (Agilent). The spectra were plotted for comparison.

For Absorption Experiment. DNA origami nanostructures at 5 nM concentration were incubated with different concentrations of Dox (62.5−500 μM) at 37 °C for 24 h. The samples were centrifuged at 15 000 rpm at 4 °C for 30 min, and then the supernatants were collected for absorption measurement at 480 nm using a microplate reader. The loading capacity was calculated as follows:[7]

$$\%\ \text{loading capacity} = (D_{in}/D_{total}) \times 100$$

when D_{in} is the final content of Dox in DNA origami nanostructures and D_{total} is the initial content of Dox in the solution

Release Capability. Each DNA origami nanostructure was incubated with 250 μM Dox at 37 °C for 24 h before centrifugation at 15 000 rpm at 4 °C for 30 min and then the supernatant was removed. The pellet was resuspended in TAE/Mg^{2+} buffer, and the mixture was incubated at 37 °C for 15 and 60 min before centrifugation at 15 000 rpm at 4 °C for 30 min and the supernatant was removed. The pellet was resuspended in TAE/Mg^{2+} buffer and the absorbance at 480 nm was measured using a microplate reader before and after incubation. The release capability of each DNA origami nanostructure was calculated as follows:

$$\%\ \text{Release} = [(A_0 - A_i)/A_0] \times 100$$

where A_0 is the initial content of Dox in DNA origami nanostructures and A_i is the content of Dox in DNA origami nanostructures after incubation

Cellular Internalization of Dox-Loaded DNA Origami Nanostructures. Cellular internalization of Dox-loaded DNA origami nanostructures on MCF-7 and MDA-MB-231 cells was examined using a fluorescence microscope. MCF-7 cells (at a density of 3500 cells/well) and MDA-MB-231 cells (at a density of 3000 cells/well) were seeded in 96-well plates and cultured overnight in DMEM supplemented with 10% FBS, 100 U/mL penicillin, and 100 μg/mL streptomycin at 37 °C in a 5% CO_2 atmosphere. For Dox-loaded DNA origami nanostructures, cells were incubated with 1 nM of Dox-loaded DNA origami nanostructures for 1 h. After washing step, cells were visualized by fluorescence microscope to determine the cellular internalization followed Dox signal compared with free dox at 10 μM.

Cell Viability Assay. Cytotoxicity of Dox-loaded DNA origami nanostructures on MCF-7 and MDA-MB-231 cells was examined using the MTT assay. MCF-7 cells (at a density of 3500 cells/well) and MDA-MB-231 cells (at a density of 3000 cells/well) were seeded in 96-well plates and cultured overnight in DMEM supplemented with 10% FBS, 100 U/mL penicillin, and 100 μg/mL streptomycin at 37 °C in a 5% CO_2 atmosphere. For Dox-loaded DNA origami nanostructures, cells were incubated with 0.5−2 nM of Dox-loaded DNA origami nanostructures for 1 h. After the incubation, the MTT assay was performed by adding MTT to get a final concentration of 0.5 mg/mL for each well and incubated at 37 °C for 3 h. Then the crystal formazan product was dissolved in DMSO and the absorbance at 540 nm was measured using a microplate reader. The percentage of cell viability can be calculated using the following equation. The absorbance of DMSO treatment was subtracted from all data:

https://doi.org/10.1021/acsabm.2c00114
ACS Appl. Bio Mater. 2022, 5, 2262−2272

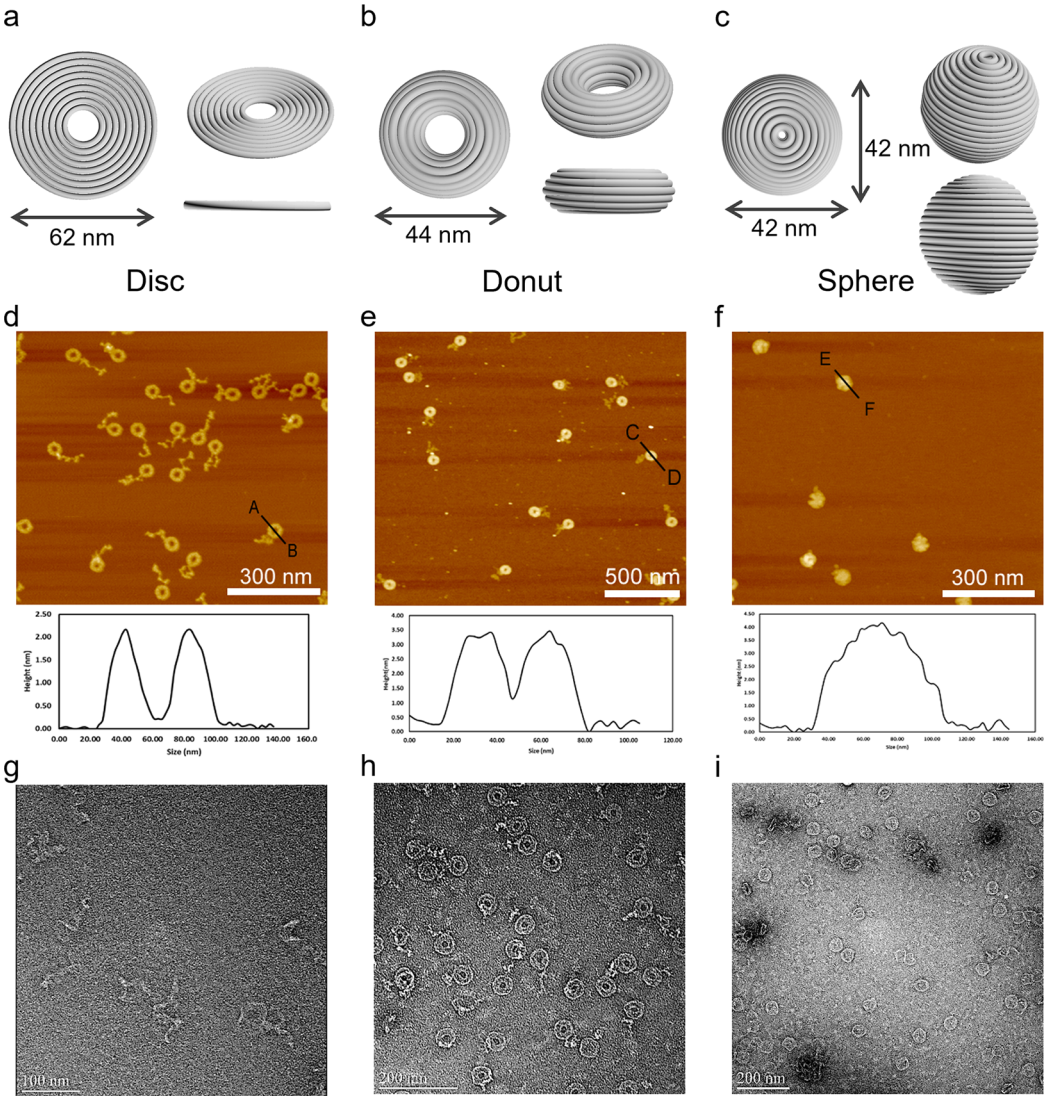

Figure 1. Structural verification of three different DNA origami nanostructures. AFM images of (a) Disc, (b) Donut, and (c) Sphere. TEM images of (d) Disc, (e) Donut, and (f) Sphere.

$$\%\ \text{cell viability} = 100 - \{[(A_{540}\ \text{of control} - A_{540}\ \text{of treated}) / A_{540}\ \text{of treated}] \times 100\}$$

where A_{540} of control is the absorbance of the cells incubated in culture media only and A_{540} of treated is the absorbance of the cell treated with DNA nanostructures.

RESULTS AND DISCUSSION

Preparation and Characterization of DNA Origami Nanostructures. Three different DNA origami nanostructures, Disc, Donut, and Sphere, were selected as model representatives for 2D and 3D DNA origami nanocarriers modified based on the previous reports[37,38,45] to determine their functional properties as targeted drug delivery vehicles (Scheme 1a). In addition, Dox was chosen as a model drug cargo that would be loaded into the annealed DNA nanostructures via intercalation (Scheme 1b). Then the cellular internalization and cytotoxicity of these Dox-loaded DNA origami nanostructures were evaluated using fluorescence microscopy and MTT assay, respectively (Scheme 1c).

As shown in Figure 1a–c, Disc is a one-helix-thick 2D planar structure with 62 nm diameter, while Donut and Sphere are 3D structures contain hollow space inside with 44 and 42 nm diameter, respectively. After the self-assembling step, DNA nanostructures were first characterized using agarose gel electrophoresis (Figure S1). Then atomic force microscopy (AFM) and transmission electron microscopy (TEM) were utilized for structure verification. The AFM images (Figure 1d–f) and TEM images (Figure 1g–i) showed that all of them were correctly formed in the desired size and shape. Interestingly, we also found that Disc structures were hardly attached onto the TEM grid leading to poor TEM images. This means that DNA nanostructures that are 2D planar structures with one-layered helix thick should be better characterized via AFM than TEM. The densely packed 3D DNA nanostructures are fine with both AFM and TEM as we can see with Donut nanostructures. For 3D-hollowed Sphere nanostructures, most of them were shown as a closed sphere when verified by TEM, while some of them were shown as an open sphere when verified by AFM (Figure S1). This might be the fact that the AFM tip can force the structure to be in an open state as the structures are soft and hollow, and the staples that hold the structure in a closed conformation are not strong enough. Furthermore, the hydrodynamic sizes of DNA origami

https://doi.org/10.1021/acsabm.2c00114
ACS Appl. Bio Mater. 2022, 5, 2262−2272

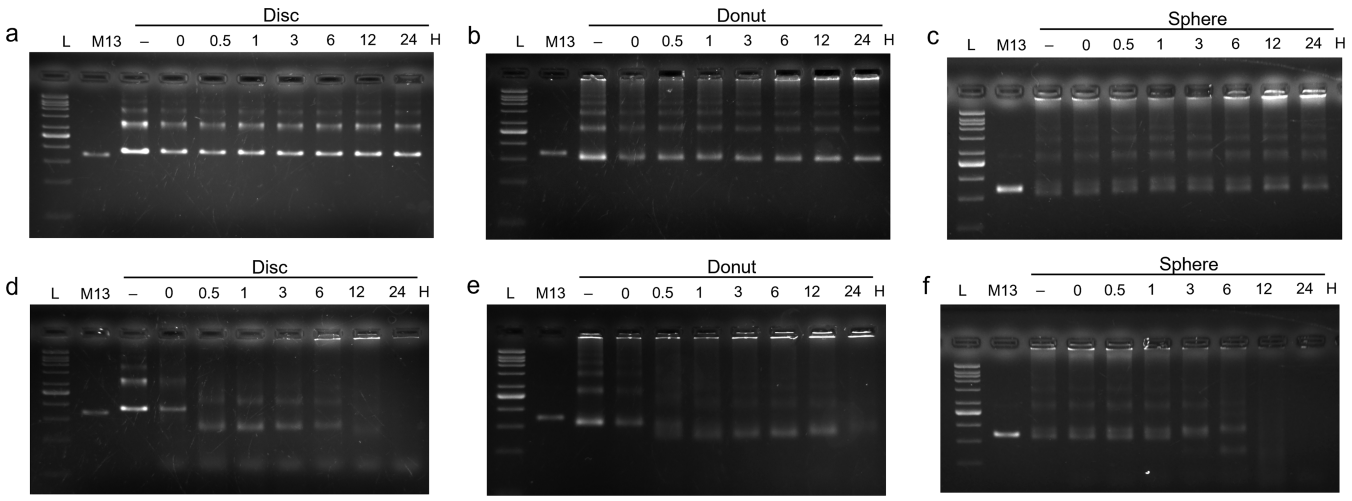

Figure 2. Stability of DNA origami nanostructures; (a) Disc, (b) Donut, and (c) Sphere in TAE/Mg2+ buffer at 37 °C and (d) Disc, (e) Donut, and (f) Sphere in DMEM containing 10% FBS at 37 °C.

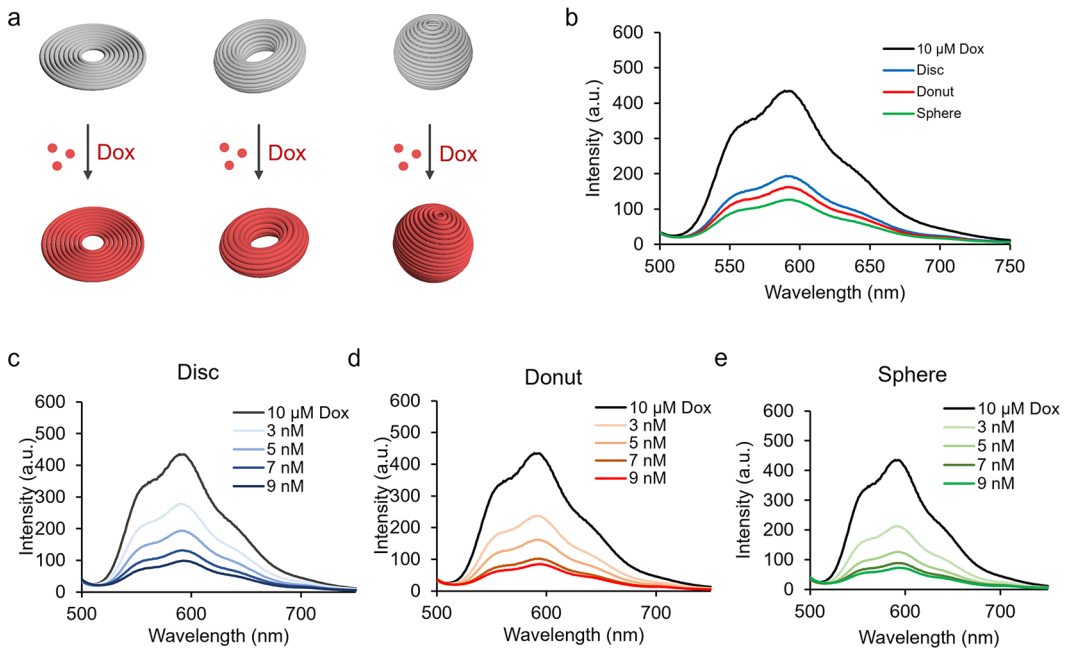

Figure 3. Drug loading of DNA origami nanostructures. (a) Diagrams of Dox loading into Disc, Donut, and Sphere. (b) Comparison of fluorescence spectra of 10 μM Dox after incubated with 5 nM concentration of Disc, Donut, and Sphere. Comparison of fluorescence spectra of 10 μM Dox after incubated with different concentrations of (c) Disc, (d) Donut, and (e) Sphere.

nanostructures before and after MUC1 aptamer modification were analyzed using dynamic light scattering (DLS). The results showed that MUC1-modified DNA origami nanostructures have larger sizes than the unmodified ones (Figure S2).

Stability of DNA Origami Nanostructures. Next, the stability of each DNA nanostructure after incubated in the annealing buffer (TAE buffer containing 12.5 mM Mg^{2+}) and cell culture media (DMEM supplemented with 10% FBS) was investigated using agarose gel electrophoresis. The results showed that when incubated in TAE/Mg^{2+} buffer at 37 °C, not much difference can be detected as shown in Figure 2a–c, and all of them could stay up to 24 h without any significant changes, consistent with the ones incubated in TAE/Mg^{2+} buffer at room temperature (Figure S3). However, after incubating these DNA nanostructures in culture media at 37 °C for 30 min, the mobilities of both Disc and Donut nanostructures in the agarose gel were changed (Figure 2d,e); this might be the components in culture media binding to DNA nanostructures and resulting in a gel mobility shift. In comparison, Sphere nanostructures in closed conformation converted into open conformation after 3 h of incubation in the media (Figure 2f). In addition, Sphere nanostructures completely disappeared after 12 h of incubation, whereas Disc and Donut nanostructures were gradually degraded after 12 and 24 h, respectively. It has been obviously shown that cell culture media can affect the stabilities of these DNA origami nanostructures as they contain many kinds of proteins and enzymes, especially nucleases. At room temperature, only Sphere nanostructures can survive up to 24 h, while Donut and Disc nanostructures changed their mobilities in agarose gel after being incubated for 6 and 3 h, respectively (Figure S3). However, the physiological temperature should be around at

https://doi.org/10.1021/acsabm.2c00114
ACS Appl. Bio Mater. 2022, 5, 2262–2272

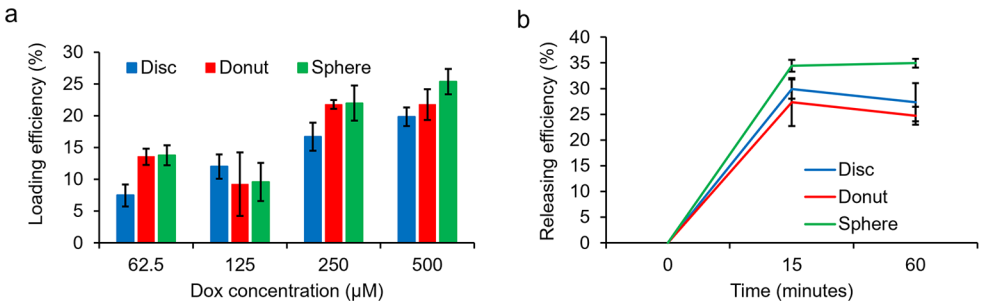

Figure 4. (a) Capacities of Dox loading and (b) release of these DNA origami nanostructures.

37 °C. The stability of these DNA nanostructures was also examined in DMEM at 37 °C, and the results showed that among three DNA origami nanostructures, Donut nanostructures exhibit the highest stability in DMEM at 37 °C. This finding is consistent with the previous reports that the stability of DNA nanostructures in low Mg^{2+} solution depends on the design of the DNA nanostructures.[56,57] This is also in agreement with previous reports that more densely packed DNA origami nanostructures are more resistant to degradation.[47,53]

Drug Loading and Releasing Capability of DNA Origami Nanostructures. Drug loading is another key requirement in designing nanovehicles for drug delivery systems. Drugs could be loaded into DNA nanocarriers in several ways depending on the physical and chemical properties of drugs. Dox is widely used as a model of chemotherapeutic agents in several DNA nanocarrier studies since its planar structures can easily be loaded into the DNA nanostructures via intercalation. Loading with Dox only led to the change of gel mobility of these DNA origami nanostructures while the structural integrity of these nanostructures stayed the same (Figure S4). Previous studies showed that the intercalation of Dox into DNA helices led to the reduction of fluorescence intensity.[58,59] To study the Dox loading efficiencies of these different DNA nanostructures, DNA origami nanostructures at different concentrations were separately incubated with the same concentration of Dox (10 μM) at 37 °C for 3 h in the dark (Figure 3a) before fluorescence intensity measurement using an excitation wavelength at 470 nm and an emission wavelength at 595 nm. When the fluorescence spectra of these three DNA origami nanostructures at 5 nM concentration were compared, as shown in Figure 3b, Sphere nanostructure exhibited the highest Dox-loading efficiency while Disc nanostructures showed the lowest Dox-loading efficiency. For all DNA origami nanostructures, the fluorescence intensity decreased when the concentrations of DNA nanostructures were increased (Figure 3c–e). This trend also happens for other concentrations of DNA origami nanostructures (Figure S5). The reason for loading efficiencies of these DNA origami nanostructures might be the case that Sphere contains the highest amounts of base pairs, which is 6558 base pairs with 42.36% GC contents, while Donut and Disc contain lower numbers of base pairs as 4785 base pairs with 40% GC contents and 3588 base pairs with 42.97% GC contents, respectively. Also, this result is consistent with the previous report that Dox can be loaded into 3D DNA origami nanostructures with hollow space inside more than 2D DNA origami nanostructures.[7]

To study the release capability of each DNA origami nanostructure, the absorption spectrophotometry was utilized for Dox loading capability determination using different Dox concentrations, ranging from 62.5–500 μM, incubated with DNA origami nanostructures (5 nM). Since self-aggregation of Dox occurred when using Dox concentration at 500 μM, the loading capacities of these DNA origami nanostructures were calculated using Dox concentration at 250 μM. The results showed that, with 250 μM Dox, the loading capacities of Disc, Donut, and Sphere are 16.69 ± 2.20%, 21.76 ± 0.69%, and 21.97 ± 2.75%, respectively. The average numbers of Dox per each DNA origami nanostructure are 8345 for Disc, 10 880 for Donut, and 10 986 for Sphere. Interestingly, with Dox concentration at 125 μM, the loading capacity of DNA origami nanostructures with hollow cavities (Donut and Sphere) was reduced. However, for a planar structure like Disc, the loading capacity of the structure is concentration-dependent (Figure 4a).

The releasing capacity was also investigated using the pellets obtained from the 250 μM Dox-loading step. First, the pellets were resuspended in TAE/Mg^{2+} buffer, and the absorbance at 480 nm was measured as the amount of Dox in the DNA origami nanostructures at 0 min. After incubated at 37 °C in the dark for 15 and 60 min, the released Dox was removed using the centrifugation method. Then the pellet was resuspended in TAE/Mg^{2+} buffer and the absorbance at 480 nm was measured as the amount of Dox in the DNA nanostructures at 15 and 60 min. The rate of drug release of each DNA origami nanostructure was calculated. The results showed that Dox was burst out from DNA origami nanostructures at the very beginning for all shapes, as shown in Figure 4b. This phenomenon is similar to a previous result that after pellet was resuspended into the fresh buffer, Dox would be dramatically released out from DNA origami nanostructures until a new equilibrium is reached.[60] At 15 min, Dox was released around 30%, 27%, and 35% for Disc, Donut, and Sphere, respectively. Among these three DNA origami nanostructures, Sphere exhibited the fastest releasing rate, while Donut exhibited the slowest releasing rate. Therefore, when loading and releasing abilities were considered together, Donut could offer the highest Dox loading capacity into targeted cells.

Cellular Internalization of MUC1 Aptamer-Modified DNA Origami Nanostructures. To enhance the specificity of our DNA origami nanostructures, each DNA nanostructure was modified with five MUC1 aptamers as shown in Scheme 1a. The aptamers were designed to be conjugated at similar positions of all three origami nanostructures. MCF-7 and MDA-MB-231 cells were selected as models used for specificity determination since they are breast cancer cell

https://doi.org/10.1021/acsabm.2c00114
ACS Appl. Bio Mater. 2022, 5, 2262–2272

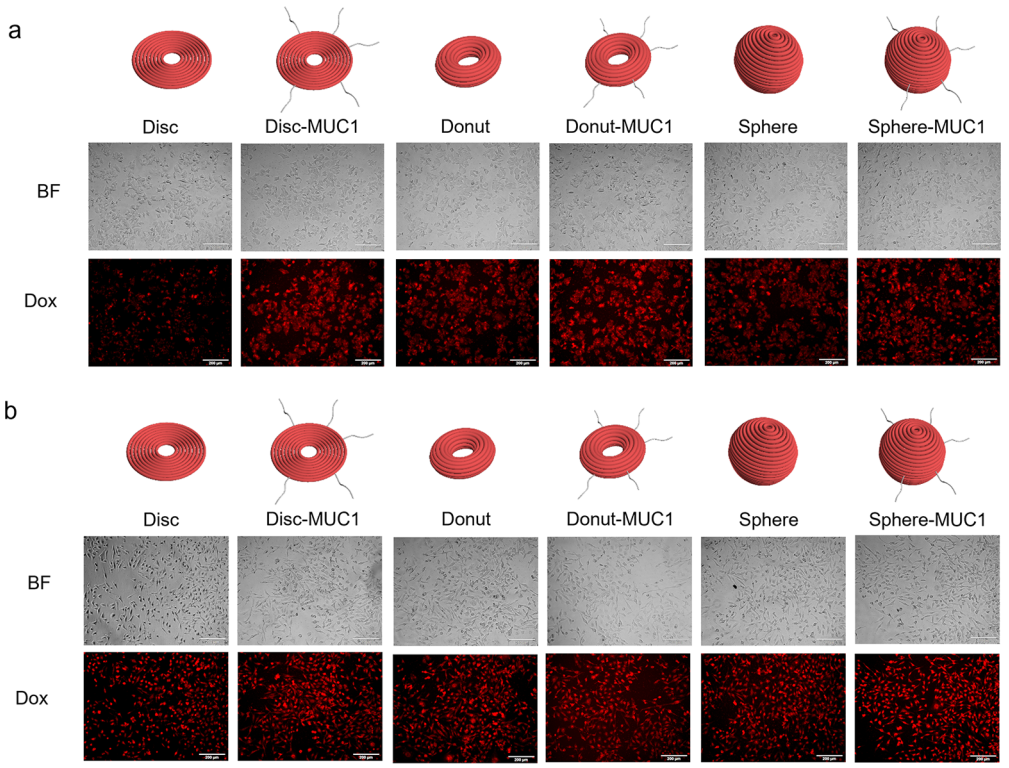

Figure 5. Cellular internalization of Dox-loaded DNA origami nanostructures with and without MUC1 aptamer into (a) MCF-7 cells and (b) MDA-MB-231 cells analyzed with the fluorescence microscopy.

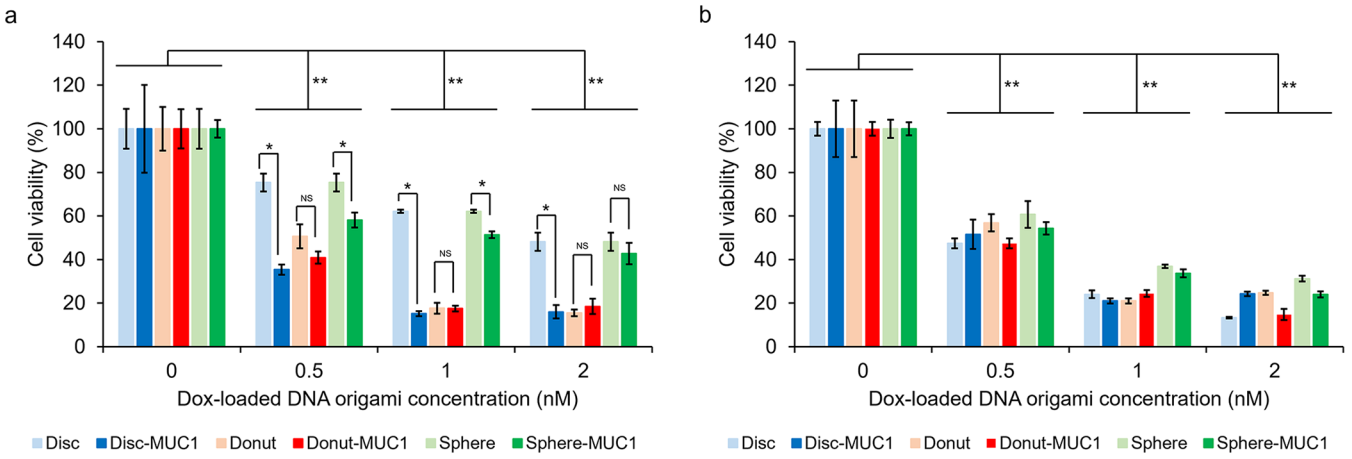

Figure 6. Cytotoxicity of Dox-loaded DNA origami nanostructures with and without MUC1-aptamer modification against (a) MCF-7 cells and (b) MDA-MB-231 cells.

lines with different Mucin 1 protein expression levels verified with Western blot and immunohistochemistry techniques (Figure S6). The results confirmed that MCF-7 cells are MUC1-positive cells and MDA-MB-231 cells are MUC1-negative cells.

Then Dox-loaded DNA origami nanostructures with and without MUC1 aptamer modification were separately treated to both MCF-7 and MDA-MB-231 cells for an hour. Cells were then visualized by fluorescence microscopy to determine the cellular internalization followed Dox signals. Compared with free Dox at 10 μM (Figure S7), the cellular uptake of Dox-loaded DNA origami nanostructures into both cell lines was significantly increased, even at 0.5 nM of Dox-loaded DNA origami nanostructures. For highly expressed Mucin 1 protein, MCF-7 cells, when compared the same shapes of DNA nanostructures with and without aptamer modification, the levels of cellular internalization into MCF-7 cells are obviously different (Figure 5a). These results confirmed that the MUC1 aptamer modification could enhance the cellular internalization into MCF-7 cells for all three DNA origami nanostructures. Among these three DNA nanostructures, Donut nanostructures showed the highest cellular internalization efficiency into MCF-7 cells both with and without aptamer modification. This might be due to the fact that Donut is more densely packed than the other two structures.[44,61] For cells with low Mucin 1 protein expression, MDA-MB-231 cells, even though DNA origami nanostructures were internalized into cells, the levels of cellular internalization of DNA origami nanostructures with

https://doi.org/10.1021/acsabm.2c00114
ACS Appl. Bio Mater. 2022, 5, 2262−2272

and without aptamer modification were similar (Figure 5b). This might be the fact that normally MDA-MB-231 cells can uptake these DNA nanocarriers better than MCF-7 cells and different geometries of the DNA nanocarriers have no effects on the cellular uptake of MDA-MB-231 cells and MUC1 aptamer modification did not affect the intracellular uptake of these DNA origami nanostructures into MDA-MB-231 cells. These results are consistent with previous studies that the cellular uptake is not only structure-type dependent but also cell-type dependent.[44,47]

Cytotoxicity of MUC1 Aptamer-Modified DNA Origami Nanostructures. The cytotoxicity of the empty DNA origami nanostructures against cancer cell lines was evaluated using the MTT assay. After incubated for 48 h, cell viability was examined. Our results showed that they were not toxic to cancer cells, which is consistent with previous studies that DNA origami nanostructures are not cytotoxic both *in vitro* and *in vivo*.[7,9,43,56,62] In addition, we also found that these DNA origami nanostructures can enhance the cell viability of MDA-MB-231 cells and MCF-7 cells (Figure S8), although the effects likely depend on cell types. Next, the cell viability of these two breast cancer cells treated with Dox-loaded DNA origami nanostructures (at 0.5−2 nM DNA origami nanostructures) with and without MUC1 aptamer modification was examined using MTT assay.

Consistent with the cellular internalization results, for MCF-7 cells, Dox-loaded DNA origami nanostructures with MUC1 aptamer modification can reduce more cell viability than Dox-loaded DNA origami nanostructures without MUC1 aptamer modification in a concentration-dependent manner (Figure 6a). For Sphere nanostructures with and without MUC1 aptamer modification, the cytotoxicity effect is not significantly increased when concentration of Dox-loaded DNA origami nanostructures increased. Interestingly, for Disc nanostructures, MUC1 aptamer modification can significantly improve the cytotoxicity effect when compared with the unmodified Disc nanostructures. However, MUC1 aptamer modification did not further improve the Dox cytotoxicity effect of Donut nanostructures. Among three DNA origami nanocarriers, Dox-loaded unmodified Donut nanostructures showed the highest cytotoxicity in MCF-7 cells.

Accordingly, for MDA-MB-231 cells, Dox-loaded DNA origami nanostructures can reduce cell viability in a concentration-dependent manner as these DNA nanocarriers could be internalized into cells (Figure 6b). However, no significant difference in Dox cytotoxicity effect against MDA-MB-231 cells could be detected between DNA origami nanostructures with and without MUC1 aptamer modification. Consequently, it seems like the modification of MUC1 aptamer onto DNA origami nanostructures does not enhance any specificity of the nanocarriers against MUC1-negative MDA-MB-231 cells.

CONCLUSIONS

In conclusion, the functional properties as targeted drug delivery nanocarriers of three DNA origami nanostructures, Disc, Donut, and Sphere, were investigated. As nanovehicles for therapeutic agent transport inside living organisms, the nanocarriers are required to be stable in physiological environments. For stability, all three shaped DNA origami nanostructures exhibited similar stability in TAE/Mg^{2+} buffer while they exhibited different stabilities in cell culture media. The results showed that Donut nanostructures offered the highest stability in DMEM supplemented with 10% FBS at 37 °C.

Although, from the fluorescence experiment, Sphere nanostructures can offer the highest Dox loading capacity due to the highest amounts of base pairs per structure, Donut nanostructures could offer the highest Dox loading efficiency when loading and release capacities were considered together.

To enhance specificity to the nanocarriers, MUC1 aptamer specific to mucin 1 proteins was selected for DNA origami nanostructure modification for evaluation the specificity against two breast cancer cell lines with significantly different levels of MUC1 protein expression; MCF-7 cells represented MUC1-positive cells and MDA-MB-231 cells represented MUC1-negative cells. Each shape of DNA origami nanostructure was modified with MUC1 aptamer at five similar positions and utilized for specificity investigation. The cellular internalization patterns of DNA origami nanostructures into MCF-7 and MDA-MB-231 cells are different. For DNA origami nanostructures without MUC1 aptamer modification, Donut nanostructures were uptake by MCF-7 cells more than Sphere and Disc nanostructures, while all three DNA nanostructures were similarly uptaken by MDA-MB-231 cells. With MUC1 aptamer modification, the cellular internalization of these three DNA origami nanostructures into MCF-7 cells was significantly enhanced when compared between the same DNA origami nanostructures. However, no significant difference could be observed with MDA-MB-231 cells for all DNA origami nanostructures.

Moreover, the cytotoxicity effect of Dox-loaded DNA origami nanostructures was evaluated. Consistent with the cellular uptake results, DNA origami nanostructures with MUC1-aptamer modification could reduce cell viability of MCF-7 cells more than DNA origami nanostructures without MUC1-aptamer modification in a concentration-dependent manner. These results confirmed that the targeting properties of DNA nanocarriers could be improved by aptamer modification. MTT assays showed that, among three DNA origami nanocarriers, Dox-loaded unmodified Donut nanostructures exerted the highest cytotoxicity in MUC1-high MCF-7 cells. However, similar cytotoxicity effects against MUC1-low MDA-MB-231 cells were observed for all shapes of DNA origami nanostructures both with and without MUC1-aptamer modification.

In summary, this study showed that among these three DNA origami nanostructures, Donut nanostructures are promising candidates for use as drug delivery vehicles due to their high stability even in cell culture media, high Dox-loading capacity, high cellular internalization, and high anticancer efficacy. Our results demonstrated that functional properties of DNA origami nanostructures as nanovehicles for drug delivery system could be achieved by appropriate structural design.

ASSOCIATED CONTENT

Supporting Information

The Supporting Information is available free of charge at https://pubs.acs.org/doi/10.1021/acsabm.2c00114.

Additional experimental methods and results; characterization of DNA origami nanostructures; hydrodynamic size analysis of DNA origami nanostructures; stability of DNA origami nanostructures; agarose gel image and AFM images of Dox-loaded DNA origami nanostructures; expression levels of mucin 1 proteins in MCF-7

https://doi.org/10.1021/acsabm.2c00114
ACS Appl. Bio Mater. 2022, 5, 2262−2272

and MDA-MB-231 cells; cellular internalization of free Dox; cytotoxicity of empty DNA origami nanostructures; sequence of staple strands (PDF)

AUTHOR INFORMATION

Corresponding Authors

Anuttara Udomprasert − *Department of Biochemistry, Faculty of Science, Burapha University, Chonburi 20131, Thailand;* orcid.org/0000-0002-5582-3085; Email: anuttara@go.buu.ac.th

Thaned Kangsamaksin − *Department of Biochemistry, Faculty of Science, Mahidol University, Bangkok 10400, Thailand*; Email: thaned.kan@mahidol.edu

Authors

Chanida Wootthichairangsan − *Department of Biochemistry, Faculty of Science, Mahidol University, Bangkok 10400, Thailand*

Ratchanee Duangrat − *Department of Biochemistry, Faculty of Science, Mahidol University, Bangkok 10400, Thailand*

Supattra Chaithongyot − *Department of Biochemistry, Faculty of Science, Mahidol University, Bangkok 10400, Thailand*

Yuwei Zhang − *Department of Chemistry, Missouri University of Science and Technology, Rolla, Missouri 65409, United States*

Rachel Nixon − *Department of Chemistry, Missouri University of Science and Technology, Rolla, Missouri 65409, United States*

Wenyan Liu − *Department of Chemistry, Missouri University of Science and Technology, Rolla, Missouri 65409, United States*

Risheng Wang − *Department of Chemistry, Missouri University of Science and Technology, Rolla, Missouri 65409, United States;* orcid.org/0000-0001-6539-1565

Mathurose Ponglikitmongkol − *Department of Biochemistry, Faculty of Science, Mahidol University, Bangkok 10400, Thailand*

Complete contact information is available at: https://pubs.acs.org/10.1021/acsabm.2c00114

Notes

The authors declare no competing financial interest.

ACKNOWLEDGMENTS

This work was financially supported by the Office of the Permanent Secretary, Ministry of Higher Education, Science, Research and Innovation (Grant No. RGNS63-141), Burapha University (A.U.), and Mahidol University (T.K.). We would like to thank the Science Innovation Facility, Faculty of Science, Burapha University and the Central Instrument Facility and the Center of Nanoimaging, Faculty of Science, Mahidol University for technical assistance and Jarinee Kongtrub for graphics. Also, the authors would like to thank the Research Unit for Sensor Innovation (RUSI) in the development and production of test kits, Burapha University for DLS measurement.

REFERENCES

(1) Renu, K.; VG, A.; PB, T. P.; Arunachalam, S. Molecular mechanism of doxorubicin-induced cardiomyopathy - An update. *Eur. J. Pharmacol.* **2018**, *818*, 241−253.

(2) Singh, N.; Nayak, J.; Sahoo, S. K.; Kumar, R. Glutathione conjugated superparamagnetic Fe_3O_4-Au core shell nanoparticles for pH controlled release of DOX. *Mater. Sci. Eng. C. Mater. Biol. Appl.* **2019**, *100*, 453−465.

(3) Maksimenko, O.; Malinovskaya, J.; Shipulo, E.; Osipova, N.; Razzhivina, V.; Arantseva, D.; Yarovaya, O.; Mostovaya, U.; Khalansky, A.; Fedoseeva, V.; Alekseeva, A.; Vanchugova, L.; Gorshkova, M.; Kovalenko, E.; Balabanyan, V.; Melnikov, P.; Baklaushev, V.; Chekhonin, V.; Kreuter, J.; Gelperina, S. Doxorubicin-loaded PLGA nanoparticles for the chemotherapy of glioblastoma: Towards the pharmaceutical development. *Int. J. Pharm.* **2019**, *572*, 118733.

(4) Tahir, N.; Madni, A.; Correia, A.; Rehman, M.; Balasubramanian, V.; Khan, M. M.; Santos, H. A. Lipid-polymer hybrid nanoparticles for controlled delivery of hydrophilic and lipophilic doxorubicin for breast cancer therapy. *Int. J. Nanomedicine.* **2019**, *14*, 4961−4974.

(5) Liu, P.; Wu, Q.; Li, Y.; Li, P.; Yuan, J.; Meng, X.; Xiao, Y. DOX-conjugated keratin nanoparticles for pH-sensitive drug delivery. *Colloids Surf. B Biointerfaces.* **2019**, *181*, 1012−1018.

(6) Qian, X.; Ge, L.; Yuan, K.; Li, C.; Zhen, X.; Cai, W.; Cheng, R.; Jiang, X. Targeting and microenvironment-improving of phenylboronic acid-decorated soy protein nanoparticles with different sizes to tumor. *Theranostics.* **2019**, *9*, 7417−7430.

(7) Jiang, Q.; Song, C.; Nangreave, J.; Liu, X.; Lin, L.; Qiu, D.; Wang, Z. G.; Zou, G.; Liang, X.; Yan, H.; Ding, B. DNA origami as a carrier for circumvention of drug resistance. *J. Am. Chem. Soc.* **2012**, *134*, 13396−13403.

(8) Song, L.; Jiang, Q.; Liu, J.; Li, N.; Liu, Q.; Dai, L.; Gao, Y.; Liu, W.; Liu, D.; Ding, B. DNA origami/gold nanorod hybrid nanostructures for the circumvention of drug resistance. *Nanoscale.* **2017**, *9*, 7750−7754.

(9) Zhang, Q.; Jiang, Q.; Li, N.; Dai, L.; Liu, Q.; Song, L.; Wang, J.; Li, Y.; Tian, J.; Ding, B.; Du, Y. DNA origami as an *in vivo* drug delivery vehicle for cancer therapy. *ACS Nano* **2014**, *8*, 6633−6643.

(10) Seeman, N. C. Nanomaterials based on DNA. *Annu. Rev. Biochem.* **2010**, *79*, 65−87.

(11) Rothemund, P. W. K. Folding DNA to create nanoscale shapes and patterns. *Nature.* **2006**, *440*, 297−302.

(12) Andersen, E. S.; Dong, M.; Nielsen, M. M.; Jahn, K.; Lind-Thomsen, A.; Mamdouh, W.; Gothelf, K. V.; Besenbacher, F.; Kjems, J. DNA origami design of dolphin-shaped structures with flexible tails. *ACS Nano* **2008**, *2*, 1213−1218.

(13) Douglas, S. M.; Marblestone, A. H.; Teerapittayanon, S.; Vazquez, A.; Church, G. M.; Shih, W. M. Rapid prototyping of 3D DNA-origami shapes with caDNAno. *Nucleic Acids Res.* **2009**, *37*, 5001−5006.

(14) Castro, C. E.; Kilchherr, F.; Kim, D. N.; Shiao, E. L.; Wauer, T.; Wortmann, P.; Bathe, M.; Dietz, H. A primer to scaffolded DNA origami. *Nat. Methods.* **2011**, *8*, 221−229.

(15) Veneziano, R.; Ratanalert, S.; Zhang, K.; Zhang, F.; Yan, H.; Chiu, W.; Bathe, M. Designer nanoscale DNA assemblies programmed from the top down. *Science.* **2016**, *352*, 1534.

(16) Noteborn, W. E. M.; Abendstein, L.; Sharp, T. H. One-pot synthesis of defined-length ssDNA for multiscaffold DNA origami. *Bioconjug Chem.* **2021**, *32*, 94−98.

(17) Praetorius, F.; Kick, B.; Behler, K. L.; Honemann, M. N.; Weuster-Botz, D.; Dietz, H. Biotechnological mass production of DNA origami. *Nature.* **2017**, *552*, 84−87.

(18) Chen, X.; Wang, Q.; Peng, J.; Long, Q.; Yu, H.; Li, Z. Self-assembly of large DNA origami with custom-designed scaffolds. *ACS Appl. Mater. Interfaces.* **2018**, *10*, 24344−24348.

(19) Stahl, E.; Martin, T. G.; Praetorius, F.; Dietz, H. Facile and scalable preparation of pure and dense DNA origami solutions. *Angew. Chem. Int. Ed.* **2014**, *53*, 12735−12740.

(20) Shaw, A.; Benson, E.; Hogberg, B. Purification of functionalized DNA origami nanostructures. *ACS Nano* **2015**, *9*, 4968−4975.

(21) Lin, C.; Perrault, S. D.; Kwak, M.; Graf, F.; Shih, W. M. Purification of DNA-origami nanostructures by rate-zonal centrifugation. *Nucleic Acids Res.* **2013**, *41*, No. e40.
(22) Voigt, N. V.; Torring, T.; Rotaru, A.; Jacobsen, M. F.; Ravnsbaek, J. B.; Subramani, R.; Mamdouh, W.; Kjems, J.; Mokhir, A.; Besenbacher, F.; Gothelf, K. V. Single-molecule chemical reactions on DNA origami. *Nat. Nanotechnol.* **2010**, *5*, 200−203.
(23) Ding, B.; Deng, Z.; Yan, H.; Cabrini, S.; Zuckermann, R. N.; Bokor, J. Gold nanoparticle self-similar chain structure organized by DNA origami. *J. Am. Chem. Soc.* **2010**, *132*, 3248−3249.
(24) Pal, S.; Deng, Z.; Wang, H.; Zou, S.; Liu, Y.; Yan, H. DNA directed self-assembly of anisotropic plasmonic nanostructures. *J. Am. Chem. Soc.* **2011**, *133*, 17606−17609.
(25) Fu, J.; Liu, M.; Liu, Y.; Woodbury, N. W.; Yan, H. Interenzyme substrate diffusion for an enzyme cascade organized on spatially addressable DNA nanostructures. *J. Am. Chem. Soc.* **2012**, *134*, 5516−5519.
(26) Halley, P. D.; Lucas, C. R.; McWilliams, E. M.; Webber, M. J.; Patton, R. A.; Kural, C.; Lucas, D. M.; Byrd, J. C.; Castro, C. E. Daunorubicin-loaded DNA origami nanostructures circumvent drug-resistance mechanisms in a Leukemia model. *Small.* **2016**, *12*, 308−320.
(27) Schuller, V. J.; Heidegger, S.; Sandholzer, N.; Nickels, P. C.; Suhartha, N. A.; Endres, S.; Bourquin, C.; Liedl, T. Cellular immunostimulation by CpG-sequence-coated DNA origami structures. *ACS Nano* **2011**, *5*, 9696−9702.
(28) Douglas, S. M.; Bachelet, I.; Church, G. M. A logic-gated nanorobot for targeted transport of molecular payloads. *Science.* **2012**, *335*, 831−834.
(29) Liu, J.; Song, L.; Liu, S.; Zhao, S.; Jiang, Q.; Ding, B. A tailored DNA nanoplatform for synergistic RNAi-/chemotherapy of multidrug-resistant tumors. *Angew. Chem., Int. Ed. Engl.* **2018**, *57*, 15486−15490.
(30) Liu, J.; Song, L.; Liu, S.; Jiang, Q.; Liu, Q.; Li, N.; Wang, Z. G.; Ding, B. A DNA-based nanocarrier for efficient gene delivery and combined cancer therapy. *Nano Lett.* **2018**, *18*, 3328−3334.
(31) Wang, Z.; Song, L.; Liu, Q.; Tian, R.; Shang, Y.; Liu, F.; Liu, S.; Zhao, S.; Han, Z.; Sun, J.; Jiang, Q.; Ding, B. A tubular DNA nanodevice as a siRNA/chemo-drug co-delivery vehicle for combined cancer therapy. *Angew. Chem., Int. Ed.* **2021**, *60*, 2594−2598.
(32) Pan, Q.; Nie, C.; Hu, Y.; Yi, J.; Liu, C.; Zhang, J.; He, M.; He, M.; Chen, T.; Chu, X. Aptamer-functionalized DNA origami for targeted codelivery of antisense oligonucleotides and doxorubicin to enhance therapy in drug-resistant cancer cells. *ACS Appl. Mater. Interfaces.* **2020**, *12*, 400−409.
(33) Wiraja, C.; Zhu, Y.; Lio, D. C. S.; Yeo, D. C.; Xie, M.; Fang, W.; Li, Q.; Zheng, M.; Van Steensel, M.; Wang, L.; Fan, C.; Xu, C. Framework nucleic acids as programmable carrier for transdermal drug delivery. *Nat. Commun.* **2019**, *10*, 1147.
(34) Yoon, S.; Rossi, J. J. Aptamers: Uptake mechanisms and intracellular applications. *Adv. Drug Deliv Rev.* **2018**, *134*, 22−35.
(35) Kufe, D. W. Mucins in cancer: function, prognosis and therapy. *Nat. Rev. Cancer.* **2009**, *9*, 874−885.
(36) Da Pieve, C.; Blackshaw, E.; Missailidis, S.; Perkins, A. C. PEGylation and biodistribution of an anti-MUC1 aptamer in MCF-7 tumor-bearing mice. *Bioconjug Chem.* **2012**, *23*, 1377−1381.
(37) Chaithongyot, S.; Chomanee, N.; Charngkaew, K.; Udomprasert, A.; Kangsamaksin, T. Aptamer-functionalized DNA nanosphere as a stimuli-responsive nanocarrier. *Mater. Lett.* **2018**, *214*, 72−75.
(38) Chaithongyot, S.; Duangrat, R.; Wootthichairangsan, C.; Hanchaina, R.; Udomprasert, A.; Kangsamaksin, T. Selective delivery of doxorubicin using the biomarker-specific, aptamer-functionalized DNA nanosphere. *Mater. Lett.* **2020**, *260*, 126952.
(39) Chang, M.; Yang, C.-S.; Huang, D.-M. Aptamer-conjugated DNA icosahedral nanoparticles as a carrier of doxorubicin for cancer therapy. *ACS Nano* **2011**, *5*, 6156−6163.
(40) Zhao, S.; Duan, F.; Liu, S.; Wu, T.; Shang, Y.; Tian, R.; Liu, J.; Wang, Z.-G.; Jiang, Q.; Ding, B. Efficient intracellular delivery of RNase A using DNA origami carriers. *ACS Appl. Mater. Interfaces.* **2019**, *11*, 11112−11118.
(41) Ko, S.; Liu, H.; Chen, Y.; Mao, C. DNA nanotubes as combinatorial vehicles for cellular delivery. *Biomacromolecules.* **2008**, *9*, 3039−3043.
(42) Sun, P.; Zhang, N.; Tang, Y.; Yang, Y.; Chu, X.; Zhao, Y. SL2B aptamer and folic acid dual-targeting DNA nanostructures for synergic biological effect with chemotherapy to combat colorectal cancer. *Int. J. Nanomed.* **2017**, *12*, 2657−2672.
(43) Zhao, Y. X.; Shaw, A.; Zeng, X.; Benson, E.; Nystrom, A. M.; Hogberg, B. R. DNA origami delivery system for cancer therapy with tunable release properties. *ACS Nano* **2012**, *6*, 8684−8691.
(44) Bastings, M. M. C.; Anastassacos, F. M.; Ponnuswamy, N.; Leifer, F. G.; Cuneo, G.; Lin, C.; Ingber, D. E.; Ryu, J. H.; Shih, W. M. Modulation of the cellular uptake of DNA origami through control over mass and shape. *Nano Lett.* **2018**, *18*, 3557−3564.
(45) Han, D.; Pal, S.; Nangreave, J.; Deng, Z.; Liu, Y.; Yan, H. DNA origami with complex curvatures in three-dimensional space. *Science.* **2011**, *332*, 342−346.
(46) Jiang, Q.; Shi, Y.; Zhang, Q.; Li, N.; Zhan, P.; Song, L.; Dai, L.; Tian, J.; Du, Y.; Cheng, Z.; Ding, B. A self-assembled DNA origami-gold nanorod complex for cancer theranostics. *Small.* **2015**, *11*, 5134−5141.
(47) Wang, P.; Rahman, M. A.; Zhao, Z.; Weiss, K.; Zhang, C.; Chen, Z.; Hurwitz, S. J.; Chen, Z. G.; Shin, D. M.; Ke, Y. Visualization of the cellular uptake and trafficking of DNA origami nanostructures in cancer cells. *J. Am. Chem. Soc.* **2018**, *140*, 2478−2484.
(48) Zeng, Y.; Liu, J.; Yang, S.; Liu, W.; Xu, L.; Wang, R. Time-lapse live cell imaging to monitor doxorubicin release from DNA origami nanostructures. *J. Mater. Chem. B* **2018**, *6*, 1605−1612.
(49) Ouyang, X.; Li, J.; Liu, H.; Zhao, B.; Yan, J.; Ma, Y.; Xiao, S.; Song, S.; Huang, Q.; Chao, J.; Fan, C. Rolling circle amplification-based DNA origami nanostructures for intracellular delivery of immunostimulatory drugs. *Small.* **2013**, *9*, 3082−3087.
(50) Kollmann, F.; Ramakrishnan, S.; Shen, B.; Grundmeier, G.; Kostiainen, M. A.; Linko, V.; Keller, A. Superstructure-dependent loading of DNA origami nanostructures with a groove-binding drug. *ACS Omega.* **2018**, *3*, 9441−9448.
(51) Jiang, D.; Ge, Z.; Im, H. J.; England, C. G.; Ni, D.; Hou, J.; Zhang, L.; Kutyreff, C. J.; Yan, Y.; Liu, Y.; Cho, S. Y.; Engle, J. W.; Shi, J.; Huang, P.; Fan, C.; Yan, H.; Cai, W. DNA origami nanostructures can exhibit preferential renal uptake and alleviate acute kidney injury. *Nat. Biomed. Eng.* **2018**, *2*, 865−877.
(52) Raniolo, S.; Croce, S.; Thomsen, R. P.; Okholm, A. H.; Unida, V.; Iacovelli, F.; Manetto, A.; Kjems, J.; Desideri, A.; Biocca, S. Cellular uptake of covalent and non-covalent DNA nanostructures with different sizes and geometries. *Nanoscale.* **2019**, *11*, 10808−10818.
(53) Palazzolo, S.; Hadla, M.; Spena, C. R.; Bayda, S.; Kumar, V.; Lo Re, F.; Adeel, M.; Caligiuri, I.; Romano, F.; Corona, G.; Canzonieri, V.; Toffoli, G.; Rizzolio, F. Proof-of-concept multistage biomimetic liposomal DNA origami nanosystem for the remote loading of doxorubicin. *ACS Med. Chem. Lett.* **2019**, *10*, 517−521.
(54) Douglas, S. M.; Dietz, H.; Liedl, T.; Hogberg, B.; Graf, F.; Shih, W. M. Self-assembly of DNA into nanoscale three-dimensional shapes. *Nature.* **2009**, *459*, 414−418.
(55) Zhang, F.; Jiang, S.; Wu, S.; Li, Y.; Mao, C.; Liu, Y.; Yan, H. Complex wireframe DNA origami nanostructures with multi-arm junction vertices. *Nat. Nanotechnol.* **2015**, *10*, 779−784.
(56) Hahn, J.; Wickham, S. F. J.; Shih, W. M.; Perrault, S. D. Addressing the instability of DNA nanostructures in tissue culture. *ACS Nano* **2014**, *8*, 8765−8775.
(57) Ramakrishnan, S.; Ijas, H.; Linko, V.; Keller, A. Structural stability of DNA origami nanostructures under application-specific conditions. *Comput. Struct. Biotechnol. J.* **2018**, *16*, 342−349.
(58) Xiao, Z.; Ji, C.; Shi, J.; Pridgen, E. M.; Frieder, J.; Wu, J.; Farokhzad, O. C. DNA self-assembly of targeted near-infrared-responsive gold nanoparticles for cancer thermo-chemotherapy. *Angew. Chem., Int. Ed.* **2012**, *51*, 11853−11857.

https://doi.org/10.1021/acsabm.2c00114
ACS Appl. Bio Mater. 2022, 5, 2262−2272

(59) Lu, S.; Zhao, F.; Zhang, Q.; Chen, P. Therapeutic peptide amphiphile as a drug carrier with ATP-triggered release for synergistic effect, improved therapeutic index, and penetration of 3D cancer cell spheroids. *Int. J. Mol. Sci.* **2018**, *19*, 2773.
(60) Ijas, H.; Shen, B.; Heuer-Jungemann, A.; Keller, A.; Kostiainen, M. A.; Liedl, T.; Ihalainen, J. A.; Linko, V. Unraveling the interaction between doxorubicin and DNA origami nanostructures for customizable chemotherapeutic drug release. *Nucleic Acids Res.* **2021**, *49*, 3048−3062.
(61) Maezawa, T.; Ohtsuki, S.; Hidaka, H.; Sugiyama, H.; Endo, M.; Takahashi, Y.; Takakura, Y.; Nishikawa, M. DNA density-dependent uptake of DNA origami-based two- or three-dimensional nanostructures by immune cells. *Nanoscale.* **2020**, *12*, 14818−14824.
(62) Mikkila, J.; Eskelinen, A. P.; Niemela, E. H.; Linko, V.; Frilander, M. J.; Torma, P.; Kostiainen, M. A. Virus-encapsulated DNA origami nanostructures for cellular delivery. *Nano Lett.* **2014**, *14*, 2196−2200.

https://doi.org/10.1021/acsabm.2c00114
ACS Appl. Bio Mater. 2022, 5, 2262−2272